Preprints of the 21st IFAC World Congress (Virtual)
Berlin, Germany, July 12-17, 2020

Feedforward Compensation of Torque Harmonics in Permanent Magnet Synchronous Machines

Oliver Dieterle * **Thomas Greiner** * **Peter Heidrich** *

* *Institute of Smart Systems and Services, Pforzheim University, Germany (e-mails: {oliver.dieterle, thomas.greiner, peter.heidrich}@hs-pforzheim.de)*

Abstract: This paper presents a method for compensation of torque ripples in electrical drives with permanent magnet synchronous machine. A standard field-oriented current control is complemented by a nonlinear feedforward control that influences the reference voltage. The compensation method has the advantage that it requires very little additional computing power and memory. Harmonic voltage components are provoked in a way that torque ripples are suppressed, while the instantaneous voltage vector magnitude of the nominal control is not changed. Additionally, an algorithm for time-saving identification of the operating point-dependent optimal compensation parameters is proposed.

Keywords: Permanent magnet synchronous machine, torque ripple compensation, feedforward control, limited phase voltage

1. INTRODUCTION

Electric drives are used in an increasing number of applications. In particular, permanent magnet synchronous machines (PMSM) are frequently used due to their high power density. In most applications there are strict requirements to torque ripple and acoustic behavior. Unfortunately, various parasitic effects in the drive have a disruptive effect on the operating behavior. While some of these effects can be reduced by design related measures, as e.g. shown for cogging torque by Zhu and Howe (2000), some others are harder to prevent in advance. The elimination of saturation induced torque ripples is probably one of the most difficult issues due to their nonlinear cause-effect relationship. If it is not possible to modify the electrical machine itself, control methods can be used to reduce the impact of parasitic effects. It is often desired to integrate the method for torque ripple compensation into an existing control system. This leads to additional requirements, as nominal control and compensation must operate in parallel.

A simple feedback control is typically not an option for the compensation of torque harmonics in most applications, since the torque is usually not measured.

Feedforward control is a more promising approach: Harmonic signals, which are intended to cause the torque ripple to disappear, are fed in the control loop. Fig. 1 gives an overview of a typical torque- and current-control structure and shows points for the injection of compensation signals at torque-, current- or voltage-level. In most cases, the bandwidth of the torque-/current-control is not sufficient to inject harmonics without amplitude- and phase-error at higher speeds and, hence, the voltage level is preferred as injection point.

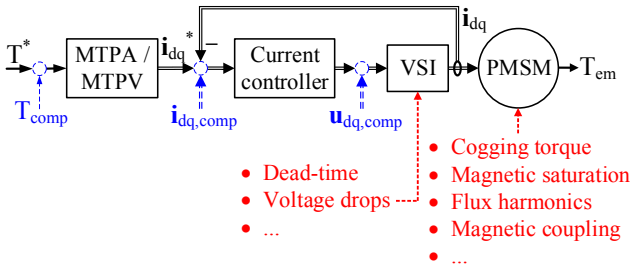

Fig. 1. Basic control loop of the electrical drive with possible intervention points for harmonic signal injection.

Another option is the model-based calculation of the optimal compensation voltages. This requires an accurate machine model, which is able to reproduce the operating point-dependent harmonic behavior. Unfortunately, in case of highly saturated PM machines it is not sufficient to consider only the cross product of magnetic flux $\boldsymbol{\psi}_{\mathrm{dq}}(t)$ and stator currents $\boldsymbol{i}_{\mathrm{dq}}(t)$ during the calculation of the electromagnetic torque with its harmonics, as shown e.g. by Bianchi and Alberti (2010). Depending on the type of machine used, a main part of the torque ripples is caused due to changes of the magnetic coenergy. As shown e.g. by Schramm et al. (2017a), a precise knowledge of the spatial distribution of permanent magnet flux as well as absolute and differential inductances at each operating point is necessary for the design of a thereon based feedforward control. The disadvantages of this method are the effort required for the modeling and the computing power needed for the online calculation of the compensation voltages. Furthermore, there can be additional parasitic effects in

⋆ This work was funded by the State of Baden-Wuerttemberg, Germany, Ministry of Science, Research and Arts within the scope of Cooperative Research Training Group.

other components of the drive, e.g. as annotated for the voltage source inverter (VSI) in Fig. 1. They must be taken into account separately.

Another option is to use a manually tuned feedforward control: Amplitude and phase shift of a compensation signal are varied in steps until an optimum is reached. The operating point dependent values of amplitude and phase shift are then stored and can be used afterwards. This must be done for various operating points that are distributed over the whole operating range. This method is e.g. used by Schramm et al. (2008) where the target is to reduce audible noise of an electrical drive. However, this process is time-consuming. The more precisely one wants to determine the ideal compensation signal, the more measurement points are needed and the longer the identification takes.

The latter problem can be avoided by an adaptive feedforward control. This way, a compensation signal is adjusted continuously until torque ripples are minimized. Such an approach is used e.g. by Benzel and Mockel (2014) to compensate gear pair vibrations.

If, however, it is desired to inject the harmonics on the voltage level, two further problems occur: First, the cross-coupling of the plant makes it difficult to compensate the torque ripples by injecting a harmonic voltage only in d- or q-direction. However, if voltages are added in both directions, amplitude and phase shift of both must be stored, which doubles the required memory. Secondly, the available voltage for the compensation is very limited in the field-weakening range. If arbitrary harmonics are added to the output of the nominal control, this can increase the output voltage temporarily and may cause a violation of the voltage limit. This issue is illustrated in Fig. 2. The violation can only be avoided by appropriate reduction of the DC component of $\boldsymbol{u}_{\mathrm{dq}}(t)$. However, this involves a reduction of the realizable maximum torque as well.

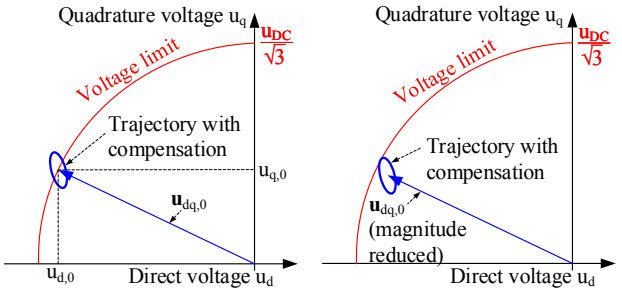

Fig. 2. Left: Violation of the voltage limit due to the superimposed harmonic components. Right: Fundamental component reduced to prevent a voltage limit violation.

This paper proposes a more resource-saving feedforward control, together with an expansion for adaptive identification of optimal operating-point-dependent compensation parameters, based on a measurement of the angular acceleration. The results are stored in LUTs and then used afterwards for a compensation of torque ripples in an application, without the need for a torque feedback or a highly accurate machine model.

2. COMPENSATION OF TORQUE RIPPLES BY HARMONIC VOLTAGE INJECTION

At first, this section presents the nominal torque- and current control (Section 2.1) as basis. Subsequently, the expansion for harmonic voltage injection (Section 2.2) is introduced. Then, the adaptive control for identification of the optimal compensation parameters is outlined (Section 2.3). At the end, an overview regarding limitations of the concept is given (Section 2.4).

2.1 Nominal Torque- and Current Control

Fig. 3 shows a block diagram of the nominal torque- and current control (the proposed feedforward control is already added, but its parts are explained later in Section 2.3). As no torque measurement is available, the torque control (labeled with MTPA / MTPV) is an open-loop control. $T^*(t)$ is the torque command. $\omega_{\mathrm{e}}(t)$ is the electrical angular velocity that is calculated from the measured rotor angle. U_{dc} is the measured DC link voltage. The torque control calculates the command signal $\boldsymbol{i}^*_{\mathrm{dq}}(t)$ for the nominal current controllers $\boldsymbol{K}(s)$ (here PI controllers are used). $\boldsymbol{u}_{\mathrm{dq}}(t)$ is the output of the nominal control, which is additionally limited to the feasible range.

As it is typical, this control loop has a limited bandwidth only, which is mainly due to a finite sample rate of the control, a considerable dead time due to computation time of the control and due to the PWM (taken into account using $\boldsymbol{G}_{\mathrm{d}}(s)$, cf. Fig. 3) and measurement noise. Therefore, the bandwidth is not sufficient for control of harmonics without amplitude- and phase error.

The impact of the harmonics, which arise in VSI and PMSM, are summarized as an unknown torque disturbance $d(t)$. It is assumed to be sinusoidal, since all dominant parasitic effects cause a deterioration of the same frequency in the considered drive. This frequency ω_{d} is a multiple of the electrical frequency of the PMSM, i.e. $\omega_{\mathrm{d}} = h\,\omega_{\mathrm{e}}$, where h is the order of the disturbance. Finally, the electrical machine is modeled by $\boldsymbol{G}_{\mathrm{EM,e}}(s)$ and $\boldsymbol{G}_{\mathrm{EM,m}}(s)$, $\boldsymbol{u}_{\mathrm{dq,ind}}(t)$ is the induced voltage due to the permanent magnets, and the load torque is considered via $T_{\mathrm{l}}(t)$.

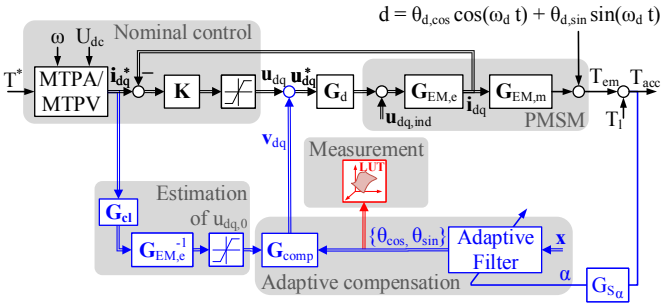

Fig. 3. Model of the closed loop with linearized harmonic voltage injection ($\boldsymbol{u}^*_{\mathrm{dq}} = \boldsymbol{u}_{\mathrm{dq}} + \boldsymbol{v}_{\mathrm{dq}}$ with the harmonic voltage $\boldsymbol{v}_{\mathrm{dq}}$) and adaption

2.2 Generation of Harmonic Voltage Components

This section presents the feedforward control for harmonic voltage injection. The goal is the compensation of the

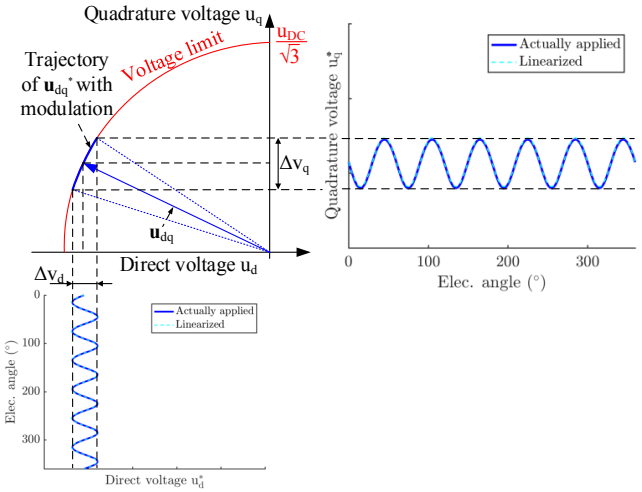

Fig. 4. Modulation of the voltage vector at an exemplary operating point where $|u_{\mathrm{d},0}| \gg 0$ and $|u_{\mathrm{q},0}| \gg 0$

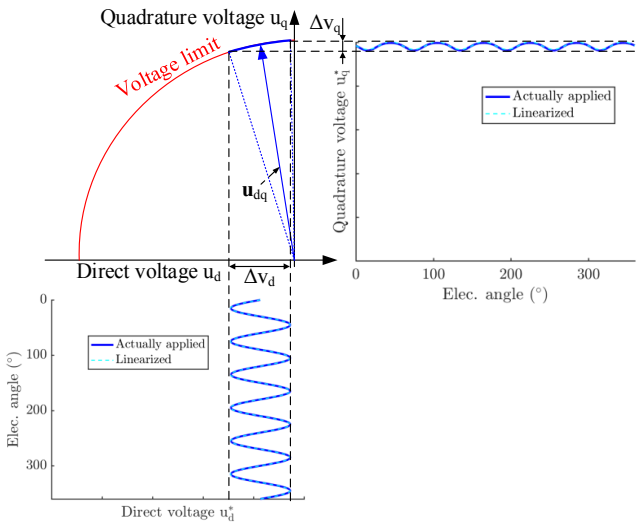

Fig. 5. Modulation of the voltage vector at an exemplary operating point where $|u_{\mathrm{d},0}|$ is small

unknown sinusoidal torque disturbance $d(t)$. Additionally, the compensation should require as little computing time and memory as possible and not lead to the voltage limit being exceeded. The compensation of the sinusoidal disturbance in the torque is achieved by provoking harmonic voltages that cause harmonic currents, which in turn lead to a compensation of the torque harmonic. This is possible under the assumption of a linear behavior of the plant in each operating point. The superposition of output of nominal control $\boldsymbol{u}_{\mathrm{dq}}(t)$ and compensation $\boldsymbol{v}_{\mathrm{dq}}(t)$ together (cf. Fig. 3) can be calculated using

$$\boldsymbol{u}^*_{\mathrm{dq}}(t) = \boldsymbol{u}_{\mathrm{dq}}(t) + \boldsymbol{v}_{\mathrm{dq}}(t) \tag{1}$$

However, in this paper it is the intention to modify the voltage vector angle $\phi_{\mathrm{u_{dq}}}(t) = \mathrm{atan2}(u_{\mathrm{q}}(t), u_{\mathrm{d}}(t))$ only, while the magnitude $|\boldsymbol{u}_{\mathrm{dq}}(t)| = \sqrt{u_{\mathrm{d}}^2(t) + u_{\mathrm{q}}^2(t)}$ is kept constant, i.e. the instantaneous values of the modified voltage vector must fulfill the constraint

$$|\boldsymbol{u}^*_{\mathrm{dq}}(t)| = |\boldsymbol{u}_{\mathrm{dq}}(t)| \tag{2}$$

Holding the voltage vector magnitude of the nominal control prevents later problems in satisfying the phase voltage constraint. As illustrated subsequently, the modulation of the voltage vector angle causes harmonics in the resulting voltage vector $\boldsymbol{u}^*_{\mathrm{dq}}(t)$, whose frequency corresponds to the modulation frequency. The subsequent explanations assume, that the steady-state voltage vector $\boldsymbol{u}_{\mathrm{dq}}(t)$ contains only negligible harmonic content. This is fulfilled if the disturbance frequency is far outside of the bandwidth of the nominal control. As discussed later, however, it is possible to partially decouple the compensation from the harmonics in $\boldsymbol{u}_{\mathrm{dq}}(t)$, which allows its use if the frequency of the torque harmonic is low.

The starting point is the equation describing the modification of the voltage vector angle

$$\phi_{\mathrm{u^*_{dq}}}(t) = \phi_{\mathrm{u_{dq}}}(t) + \underbrace{\gamma \cos(\omega_{\mathrm{d}}\, t + \delta)}_{v_{\mathrm{inj}}(t)} \tag{3}$$

where $v_{\mathrm{inj}}(t)$ is the injection signal. The optimal values for the compensation parameters, i.e. amplitude γ and phase shift δ of the injection signal, are unknown yet. The principle is illustrated in Fig. 4 and Fig. 5 for one operating points each. In both cases the output voltage of the nominal control is already at the voltage limit. The modulation causes the instantaneous manipulated voltage $\boldsymbol{u}^*_{\mathrm{dq}}(t)$ to move on a circular arc with radius $|\boldsymbol{u}_{\mathrm{dq}}(t)|$. The projection of the trajectory on the q-axis yields

$$\begin{aligned} u^*_{\mathrm{q}}(t) &= |\boldsymbol{u}_{\mathrm{dq}}(t)| \Big(\sin\left(\phi_{\mathrm{u_{dq}}}(t)\, v_{\mathrm{inj}}(t)\right) \\ &\quad + \cos\left(\phi_{\mathrm{u_{dq}}}(t)\, v_{\mathrm{inj}}(t)\right) \Big) \\ &= u_{\mathrm{q}}(t)\, \cos\left(v_{\mathrm{inj}}(t)\right) + u_{\mathrm{d}}(t)\, \sin\left(v_{\mathrm{inj}}(t)\right) \end{aligned} \tag{4}$$

For small angles, e.g. $v_{\mathrm{inj}}(t) < 15°$, (4) can be approximated as

$$\begin{aligned} u^*_{\mathrm{q}}(t) = u_{\mathrm{q}}(t) &- \frac{1}{4}\, u_{\mathrm{q}}(t)\, \gamma^2 + u_{\mathrm{d}}(t)\, \gamma\, \cos(\omega_{\mathrm{d}}\, t + \delta) \\ &- \frac{1}{4}\, u_{\mathrm{q}}(t)\, \gamma^2\, \cos(2\,\omega_{\mathrm{d}}\, t + 2\,\delta) \end{aligned} \tag{5}$$

and consequently

$$\begin{aligned} v_{\mathrm{q}}(t) = &- \frac{1}{4}\, u_{\mathrm{q}}(t)\, \gamma^2 + u_{\mathrm{d}}(t)\, \gamma\, \cos(\omega_{\mathrm{d}}\, t + \delta) \\ &- \frac{1}{4}\, u_{\mathrm{q}}(t)\, \gamma^2\, \cos(2\,\omega_{\mathrm{d}}\, t + 2\,\delta) \end{aligned} \tag{6}$$

Unfortunately, the induced harmonic $v_{\mathrm{q}}(t)$ is not purely sinusoidal but contains a DC component and a component with order $2h$ as well. This can be derived for $v_{\mathrm{d}}(t)$ in the same way. The DC component is no problem anyways, since it will be corrected by the nominal controller. The component with double frequency can cause a distortion in the torque with same frequency. However, since the complex resistance for this frequency is significantly higher, the current harmonic caused by it is low. Neglecting these components, it turns out

$$v_{\mathrm{q}}(t) \approx u_{\mathrm{d}}(t)\, \gamma\, \cos(\omega_{\mathrm{d}}\, t + \delta) \tag{7}$$

$$v_{\mathrm{d}}(t) \approx -u_{\mathrm{q}}(t)\, \gamma\, \cos(\omega_{\mathrm{d}}\, t + \delta) \tag{8}$$

The accuracy of the approximation can be observed exemplarily in Fig. 4 and Fig. 5, when comparing the "Actually applied" curve and the "Linearized" curve that is calculated using (7) and (8).

If $u_\mathrm{d}(t)$ and $u_\mathrm{q}(t)$ are considered as parameters that are constant or slowly varying, which is the case in static operating points and under the assumptions that the bandwidth of the nominal control is distinctly smaller than the frequency of the considered harmonic, there is a linear relation

$$\boldsymbol{V}_\mathrm{dq}(s) = \boldsymbol{G}_\mathrm{comp}(s)\, V_\mathrm{inj}(s) \tag{9}$$

with the Laplace transforms $V_\mathrm{inj}(s)$ and $\boldsymbol{V}_\mathrm{dq}(s)$ of $v_\mathrm{inj}(t)$ and $\boldsymbol{v}_\mathrm{dq}(t)$ respectively and with

$$\boldsymbol{G}_\mathrm{comp}(s) = \begin{bmatrix} -u_\mathrm{q} \\ u_\mathrm{d} \end{bmatrix} \tag{10}$$

to describe the impact of the proposed compensation (cf. Fig. 3). An even better alternative is to replace $u_\mathrm{d}(t)$ and $u_\mathrm{q}(t)$ in (7) by estimated values $\hat{\boldsymbol{u}}_\mathrm{dq,0}(t)$ for its DC component:

$$\hat{\boldsymbol{u}}_\mathrm{dq,0}(t) = \mathrm{sat}\left(\mathcal{L}^{-1}\left\{\hat{\boldsymbol{G}}^{-1}_\mathrm{EM,e}(s)\, \boldsymbol{G}_\mathrm{cl}(s)\, \boldsymbol{I}^*_\mathrm{dq}(s)\right\}\right) \tag{11}$$

where $\boldsymbol{G}_\mathrm{cl}(s)$ are the nominal dynamics of the current control loop, $\boldsymbol{I}^*_\mathrm{dq}(s)$ is the Laplace transform of $\boldsymbol{i}^*_\mathrm{dq}(t)$ and $\mathrm{sat}(\cdot)$ is the nonlinear function to limit the output voltage to the realizable range. This reduces the mutual influence between the nominal control and the harmonic voltage injection, especially if the frequency of the torque ripple falls in the bandwidth of the nominal control.

The compensation parameters $\{\gamma,\, \delta\}$ can now be used for manipulating the harmonics in $\boldsymbol{u}^*_\mathrm{dq}$. The magnitude of $\boldsymbol{u}_\mathrm{dq}$ remains constant as desired.

2.3 Adaptive Identification of Optimal Amplitude and Phase Shift of the Compensation Signal

The next step is to identify the optimal values for the compensation parameters γ and δ that lead to a suppression of the torque ripple. They depend on the operating point $\{T^*, \omega_\mathrm{e}, U_\mathrm{dc}\}$. One option to identify them, is to manually adapt γ and δ in an iterative manner, until a minimum is reached for the harmonic amplitude in the torque. However, this process is time-consuming. Therefore, a method for fast identification of the optimal parameters is proposed. A narrowband filter is adapted automatically in dependence on a measured error signal that correlates well with the electromagnetical torque of the PMSM. Note that it is required that the load does not have an perceptible influence on the torque harmonic to be cancelled. Torque harmonics can be captured directly via a torque sensor or indirectly via the angular speed or the angular acceleration. However, the bandwidth of a typical torque measurement using a torque sensor with torsion shaft is limited to lower frequencies and, due to a typically large inertia, the transfer behavior from torque to angular speed is only beneficial in a small frequency range as well. However, electromagnetic torque and angular acceleration correlate well over a wide frequency range. Hence, the angular acceleration is used as error signal here. At the test bench it can be measured with a piezoelectric accelerometer, which rotates on the shaft of the PMSM, as e.g. proposed by Schramm et al. (2017b). Fig. 3 shows a block diagram of the proposed control. The signal d represents an unknown torque harmonic with frequency ω_d to be compensated. The origin of the torque ripple is not of importance here, since the compensation is automatically adapted in a way that their impact on the measured error signal is canceled. For this purpose, an adaptive narrowband filter with output

$$v_\mathrm{inj}(t) = \underbrace{\left[\cos(\omega_\mathrm{d}\, t)\ \sin(\omega_\mathrm{d}\, t)\right]}_{\boldsymbol{x}(t)^\top} \underbrace{\begin{bmatrix}\theta_\mathrm{cos}(t) \\ \theta_\mathrm{sin}(t)\end{bmatrix}}_{\boldsymbol{\theta}(t)} \tag{12}$$

is adjusted continuously to drive the error (i.e. the harmonic in the measured angular acceleration $\alpha(t)$) towards zero. The procedure for finding the optimal filter weights is explained e.g. by Maier et al. (2011). It is outlined in brief subsequently.

The target is to minimize the squared error $\alpha^2(t)$. This is done by adapting the states $\theta(t)$ in direction of the negative gradient, which itself is a function of the adaptive states:

$$\dot{\boldsymbol{\theta}}(t) = -\mu \left(\frac{\partial \alpha^2(t)}{\partial \boldsymbol{\theta}(t)}\right)^\top \tag{13}$$

The parameter μ is used to tune the gain of the adaption.

For the next step, the parts of the model that lie on the way between output of the linearized model of the compensation $\boldsymbol{G}_\mathrm{comp}(s)$ and the error signal are summarized as so-called secondary path system:

$$\boldsymbol{S}(s) = \boldsymbol{G}_{\mathrm{S}_\alpha}(s)\, \boldsymbol{G}_\mathrm{EM,m}(s)\, \boldsymbol{G}_\mathrm{EM,e}(s)\, \boldsymbol{G}_\mathrm{d}(s)\, \boldsymbol{G}_\mathrm{comp}(s) \tag{14}$$

The secondary path system distorts amplitude and phase of the filter output signal. It must be considered in the adaption law, since it can worsen the behavior of the adaption and cause instability in the worst case.

Under the assumptions that the gain of the adaption is chosen appropriately low and, therefore, that the filter weights change slowly compared to the other variables in the system, the gradient (13) can be evaluated assuming constant weights. With the steady-state error signal

$$\alpha_\mathrm{ss}(t) = \boldsymbol{x}^\top(t)\, \boldsymbol{S}_\mathrm{ss}(\omega_\mathrm{d})\, (\boldsymbol{\theta}_\mathrm{d} + \boldsymbol{\theta}(t)) \tag{15}$$

where $\boldsymbol{S}_\mathrm{ss}(\omega_\mathrm{d})$ is the frequency response of $\boldsymbol{S}(\omega_\mathrm{d})$ and after normalizing, the gradient is

$$\begin{aligned} \dot{\boldsymbol{\theta}}(t) = &-2\,\mu\, \frac{1}{||\hat{\boldsymbol{S}}^\top_\mathrm{ss}(\omega_\mathrm{d})\, \boldsymbol{x}(t)\, \boldsymbol{x}^\top(t)\, \hat{\boldsymbol{S}}_\mathrm{ss}(\omega_\mathrm{d})||_\mathrm{F}} \\ &\hat{\boldsymbol{S}}^\top_\mathrm{ss}(\omega_\mathrm{d})\, \boldsymbol{x}(t)\, \alpha(t) \\ = &-2\,\mu\, \hat{\boldsymbol{S}}^+_\mathrm{ss}(\omega_\mathrm{d})\, \boldsymbol{x}(t)\, \alpha(t) \end{aligned} \tag{16}$$

where $||\cdot||_\mathrm{F}$ is the Frobenius norm and $(\cdot)^+$ is the Moore-Penrose inverse. $\hat{\boldsymbol{S}}^+_\mathrm{ss}(\omega_\mathrm{d})$ is the filter of the adaption.

For the calculation of $\hat{\boldsymbol{S}}^+_\mathrm{ss}(\omega_\mathrm{d})$, all parts of the secondary path are approximated using LTI systems: $\boldsymbol{G}_\mathrm{comp}(s)$ is the linearized voltage compensation strategy that was already derived in Section 2.2. The delay due to calculation time and PWM is modeled by

$$\boldsymbol{G}_\mathrm{d}(s) = e^{-sT_\mathrm{d}} \boldsymbol{I}_2 \tag{17}$$

where T_d is the overall dead time and $\boldsymbol{I}_2$ is the 2x2 identity matrix. The PMSM is modeled using

$$\boldsymbol{A} = \begin{bmatrix} -\frac{R_\mathrm{s}}{L_\mathrm{d}} & \omega_\mathrm{e}\frac{L_\mathrm{q}}{L_\mathrm{d}} \\ -\omega_\mathrm{e}\frac{L_\mathrm{d}}{L_\mathrm{q}} & -\frac{R_\mathrm{s}}{L_\mathrm{q}} \end{bmatrix} \qquad \boldsymbol{B} = \begin{bmatrix} \frac{1}{L_\mathrm{d}} & 0 \\ 0 & \frac{1}{L_\mathrm{q}} \end{bmatrix} \tag{18}$$

$$\hat{\boldsymbol{G}}_{\mathrm{EM,e}}(s) = (s\boldsymbol{I}_2 - \boldsymbol{A})^{-1}\,\boldsymbol{B} \tag{19}$$

where $\boldsymbol{A}$ is the system matrix and $\boldsymbol{B}$ is the input matrix. The relation between current and torque is approximated using the torque constant $k_\mathrm{T} = 1.5\,N_\mathrm{p}\,\psi_\mathrm{p}$ and

$$\hat{\boldsymbol{G}}_{\mathrm{EM,m}}(s) = \begin{bmatrix} 0 \\ k_\mathrm{T} \end{bmatrix} \tag{20}$$

The model of the PMSM is adapted to the current operating point by adapting $\{L_\mathrm{d},\ L_\mathrm{q},\ \psi_\mathrm{p}\}$ according to the load. This leads to an accurate approximation of the nonlinear behavior in each operating point. Since a closed loop control is used, it is sufficient to use a linearized model of the plant at this point. The model must be accurate enough that the gain of the adaption can be chosen sufficiently high and that the adaption will not become unstable.

Furthermore, $\boldsymbol{G}_{\mathrm{S}_\alpha}(s)$ is an approximation for the transfer behavior between electromagnetic torque and measured angular acceleration. It was identified experimentally in advance and, in the relevant frequency range from approximately 100 to 1600 Hz, it can be approximated accurately using a second order system with single zero $s_1 = -35954$ and poles $s_{1,2} = -19.6 \pm \mathrm{j}\,6746.2$. Note that this transfer behavior depends on the mechanical test bench setup, including the angular acceleration sensor and the PMSM itself.

The adaptive filter is proposed to determine the optimal compensation parameters on the test bench only. For use in an application where no accurate measurement of the angular acceleration is available typically, it is proposed to store the operating point-dependent compensation parameters in LUTs and to use them in a feedforward control as shown in Fig. 6. The recording of the compensation parameters is outlined in Fig. 3. Note that the relation between the adaptive states $\{\theta_\mathrm{cos}, \theta_\mathrm{sin}\}$ and the compensation parameters $\{\gamma, \delta\}$ is

$$\gamma = \sqrt{\theta_\mathrm{cos}^2 + \theta_\mathrm{sin}^2} \tag{21}$$

$$\delta = -\mathrm{atan2}(\theta_\mathrm{sin}, \theta_\mathrm{cos}) \tag{22}$$

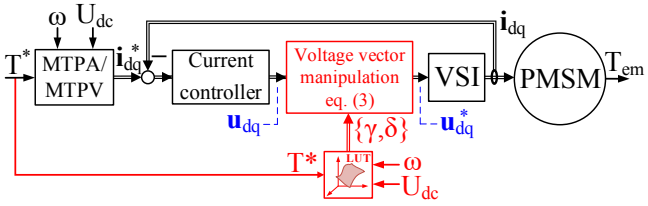

Fig. 6. Control loop of Fig. 1 complemented by the feedforward control for compensation of torque ripples.

2.4 Additional considerations and limitations

Since the nominal control is not decoupled from the harmonic voltage injection, they influence each other. Therefore, the gain μ of the adaption must be sufficiently low to ensure a stable operation and to limit the influence of the adaption during dynamic transitions. The compensation (as it is proposed) is a suitable addition for current controls with low bandwidth and for higher operating speeds mainly. In case of large bandwidth or small speed, the nominal control will increasingly counteract against the current harmonics that are induced using the harmonic voltage injection. It is also important to note that the set of optimal compensation parameters is a function of the nominal current control. Hence, it is only optimal as long as the nominal control is not changed. A decoupling from the nominal control, however, would require an increased calculation effort when used in an application, which was avoided here.

Due to the transfer behavior (10) of the voltage vector manipulation it can not be guaranteed that a specific harmonic in the torque can be suppressed completely in each operating point. One must consider that the amplitude of the harmonic that is induced in d- resp. q-direction is small, if the average voltage component in q- resp. d-direction is small (e.g. in case of small load in the base speed range, the compensation cannot influence the voltage in q-direction, cf. in Fig. 5 where $|u_{\mathrm{d},0}|$ is small). As a consequence, the amplitude of the compensation signal resp. the amplitudes of the induced voltage- and current harmonics can get too large. In this case, the plant may behave nonlinear. This can even cause the adaptation to become unstable. Two measures are proposed to consider this: First, an additional logical control should turn off the adaption, as long as the drive is operated in a region where the compensation is not able to work properly. Secondly, it is proposed to limit the amplitude γ (i.e. the output of the adaption) to a maximum value (e.g. 15°) and add an anti-windup, which limits the states when the amplitude becomes too large. With active limitation, however, the torque ripple will not be minimized.

If the harmonic with order h in the torque is suppressed, then the harmonic with order $2h$ can be amplified due to the injection of the voltage harmonics. However, its absolute amplitude is likely to be low compared to the initial amplitude of order h.

3. EVALUATION

For the evaluation, a PMSM with surface mounted magnets is used. It has 12 tooth-coils that are connected in 3-phase star connection. Some additional parameters of the test setup are summarized in Table 1. A sketch of the mechanical test bench setup and the maximum torque-speed-curve are shown in Fig. 7.

In the utilized PMSM, mainly harmonics of 6th electrical order occur at higher loads due to magnetic saturation. Additionally, the VSI causes 6th order harmonics due to the dead time. Both effects cause a dominant 6th harmonic in the electromagnetical torque that depends on the load and, due to the parasitic effects of the VSI, on the DC link voltage level. The target is to compensate this order.

Table 1. Parameters of the test setup.

Parameter	Symbol	Value
Number of pole pairs	N_p	4
Maximum phase current amplitude	$I_\mathrm{ph,max}$	113 A
Bandwidth of the nominal control	$f_{\ 3\,\mathrm{dB}}$	160 Hz
Controller period	T_ctrl	(16 kHz) $^{-1}$
Control dead time	$T_\mathrm{d,ctrl}$	$1.5 \cdot$ (16 kHz)-1
VSI dead time	$T_\mathrm{d,VSI}$	1 µs
DC link voltage	U_dc	12 V

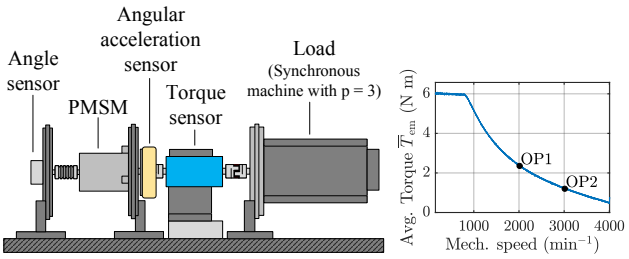

Fig. 7. Left: Sketch of the test bench setup. Right: Measured curve showing the maximum torque over speed.

As example, the optimal compensation parameters are determined for the operating point OP1 = $\{2.5\,\mathrm{N\,m}, 2000\,\mathrm{min}^{-1}\}$ (cf. Fig. 7). This is done in an iterative manner first. The compensation parameter γ is varied in the range $0.5° \leq \gamma \leq 10°$ in steps of 0.5° while δ is varied in the range $0° \leq \delta < 360°$ in steps of 20°, i.e. there are 360 measurement points. The steps must be chosen small enough that the optimum parameters can be read off easily later and the total measuring time for all steps is still not too long. The results for the amplitude and the phase shift of the 6th harmonic in the measured angular acceleration α are shown in Fig. 8. Here and in subsequent graphs, the amplitude of the angular acceleration is normalized with respect to the full measurement range of the utilized sensor. With $\{\gamma = 3°, \delta = 280°\}$, the minimum is reached for this operating point.

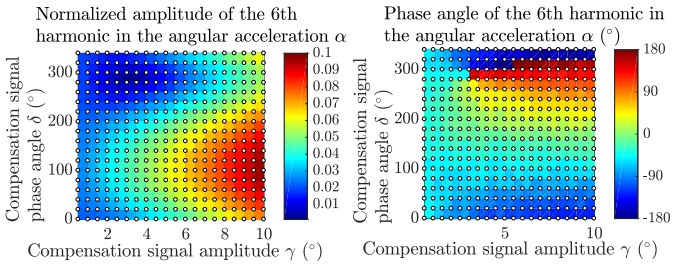

Fig. 8. Measured results for the 6th harmonic in the angular acceleration at OP1 (cf. Fig. 7) in dependence on the compensation parameters. The dots denote the measured samples.

In the next step, the adaptive filter is used for a faster identification of the optimal compensation parameters at the same operating point. Fig. 9 shows the transient response of the states of the filter. The 6th harmonic is canceled completely, as soon as the states reach the steady-state. In the steady state, the harmonic content of the angular acceleration signal results from other harmonics and measurement noise. The values of the states in steady-state correspond to a compensation signal amplitude of

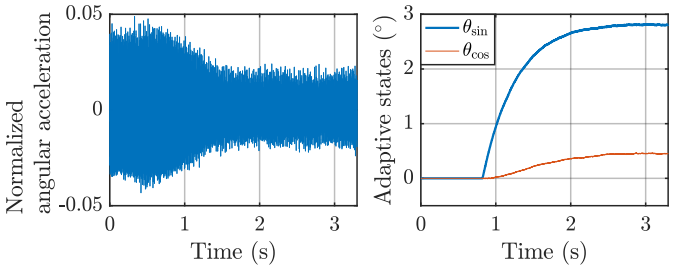

Fig. 9. Measured transient response of the angular acceleration (left) and the states (right) when the adaption is activated at OP1 (cf. Fig. 7)

2.84° and a phase shift of 279.17°. This matches the result of the iterative identification.

At last, Fig. 10 shows the output voltages of the control $\boldsymbol{u}^*_\mathrm{dq}(t)$, phase currents $\boldsymbol{i}_\mathrm{dq}(t)$ and angular acceleration α for the operating point OP2 = $\{1.3\,\mathrm{N\,m}, 3000\,\mathrm{min}^{-1}\}$ (cf. Fig. 7) for the case without compensation and with active compensation. As it can be seen in the amplitude response, the 6th harmonic in the angular acceleration is vanished completely, when the compensation is used. Furthermore, the trajectory of $u^*_\mathrm{dq}(t)$ is shown: When the compensation is active, the maximum instantaneous voltage magnitude of the control is slightly increased. This results mainly from the nominal controllers that are not decoupled from the harmonic voltage injection here. However, the voltage magnitude increase is small.

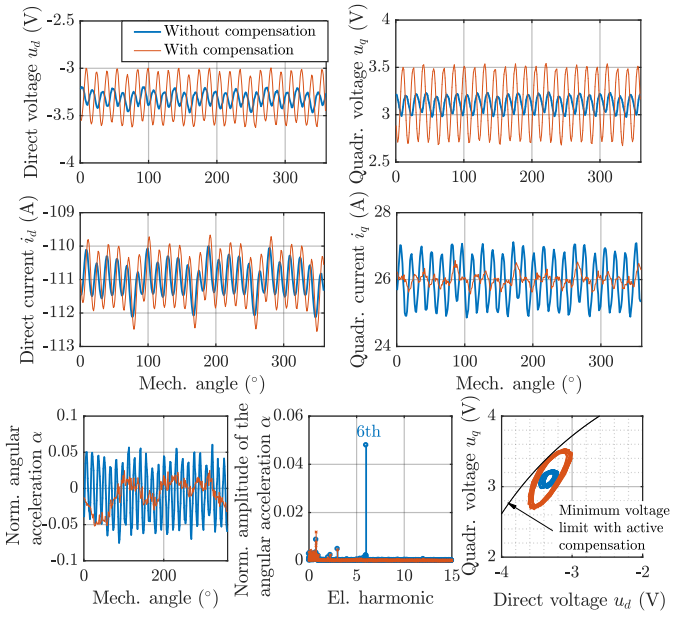

Fig. 10. Comparison of the measured behavior at OP2 (cf. Fig. 7) without compensation and with active compensation.

3.1 Decoupling of Nominal Control and Harmonic Injection

Finally, it is shown how the control behaves when nominal control and harmonic voltage injection are decoupled. For this purpose the harmonic currents, which are caused by the harmonic voltage injection, must be estimated. These harmonic currents are subtracted from the measured currents and thus made invisible for the nominal control.

The results in this section are obtained by simulations. This offers the advantage that no undesired harmonic disturbances occur, which are unavoidable on the test bench due to parasitic effects (e.g. voltage harmonics due to the dead time of the inverter). As long as the phase currents show any harmonic content, which is the typical case at the testbench, the nominal control will counteract against them and the magnitude of the voltage vector of the nominal control will not be completely constant, as constituted in Fig. 4 and in Fig. 5. For this reason, a fundamental wave model is used for the subsequent tests, which is only complemented by a single sinusoidal disturbance

$$d(t) = \hat{d}\,\sin(h\,\phi_\mathrm{e}(t)) \tag{23}$$

with $\hat{d} = 40\,\mathrm{mN\,m}$ and $h = 6$ that acts directly on the torque, as shown in Fig. 3. As already mentioned, the decoupling is mainly needed when the operating speed is low or when the bandwidth $f_{-3\,\mathrm{dB}}$ of the nominal control is large. For this reason, the tests were conducted choosing $f_{-3\,\mathrm{dB}} = 1.2\,\mathrm{kHz}$. Figure 11 shows a comparison between results with and without decoupling at $T^* = T^*_\mathrm{max}$ and $n_\mathrm{mech} = 1000\,\mathrm{min}^{-1}$. In both cases, $d(t)$ is canceled completely. However, without decoupling a higher phase voltage magnitude is required partially and it takes distinctly longer until the steady-state is reached.

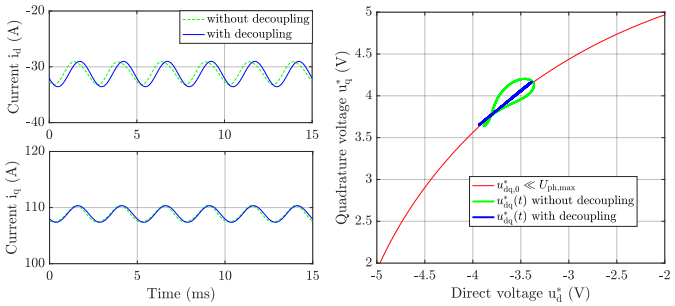

Fig. 11. Comparison of the simulation results in steady-state with and without decoupling at $T^* = T^*_\mathrm{max}$ and $n_\mathrm{mech} = 1000\,\mathrm{min}^{-1}$

In Fig. 12, results at $T^* = T^*_\mathrm{max}$ and a very low rotational speed of $n_\mathrm{mech} = 200\,\mathrm{min}^{-1}$ are depicted. Without decoupling, the control is not able to cancel the disturbance. Due to the counteracting of the nominal control, the closed loop even becomes unstable, if the amplitude of the harmonic injection is not limited to a maximum value as explained in Section 2.4. By decoupling nominal control and harmonic voltage injection, the closed loop remains stable and $d(t)$ is canceled completely.

However, as can be seen in Fig. 12 as well, the harmonic d-current, which is caused by the voltage vector manipulation, has a large amplitude in this scenario, even if the amplitude of the disturbance $d(t)$ is relatively low. This is an inherent drawback of the method that becomes visible at this operating point. I.e. in case of slow rotational speed and/or large bandwidth of the nominal control either the additional losses must be accepted, or the harmonic voltage injection must be switched off. Though, in contrast to the results shown in Fig. 10, the magnitude of the voltage vector remains constant using the decoupling.

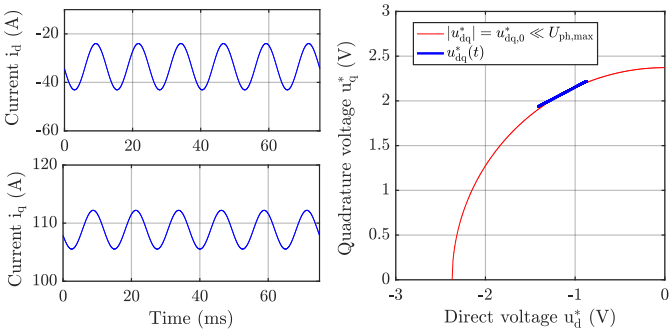

Fig. 12. Simulation result in steady-state with decoupling at $T^* = T^*_\mathrm{max}$ and $n_\mathrm{mech} = 200\,\mathrm{min}^{-1}$

4. CONCLUSION

The presented harmonic voltage injection is a resource-efficient method to suppress a specified harmonic in the electromagnetic torque. The optimal compensation parameters can be identified using an adaptive filter together with the measured angular acceleration as error signal. The results of the identification can be stored in LUTs and used in an application subsequently. The sensor for measuring the angular acceleration is no longer required then. If an increased computing effort in the application is not a problem, it would also be possible to decouple nominal control and harmonic voltage injection to enable an improved compliance with a limited voltage margin.

REFERENCES

Benzel, T. and Mockel, H.A. (2014). Active control of gear pair vibration with an electronically commutated motor as actuator. In *2014 4th International Electric Drives Production Conference (EDPC)*, 1–6. doi: 10.1109/EDPC.2014.6984426.

Bianchi, N. and Alberti, L. (2010). Mmf harmonics effect on the embedded fe analytical computation of pm motors. *IEEE Transactions on Industry Applications*, 46(2), 812–820. doi:10.1109/TIA.2010.2041098.

Maier, S., Bals, J., and Bodson, M. (2011). Periodic disturbance rejection of a pmsm with adaptive control algorithms. In *2011 IEEE International Electric Machines & Drives Conference (IEMDC)*, 1070–1075. IEEE. doi:10.1109/IEMDC.2011.5994749.

Schramm, A., Sworowski, E., and Roth-Stielow, J. (2017a). Compensation of torque ripples in permanent magnet synchronous machines up to the field weakening range. In *2017 7th International Electric Drives Production Conference (EDPC)*, 1–8. IEEE. doi: 10.1109/EDPC.2017.8328154.

Schramm, A., Sworowski, E., and Roth-Stielow, J. (2017b). Methods for measuring torque ripples in electrical machines. In *2017 IEEE International Electric Machines and Drives Conference (IEMDC)*, 1–8. IEEE. doi: 10.1109/IEMDC.2017.8002175.

Schramm, S., Sihler, C., Hemmelmann, J., and Roesner, R. (2008). *Gearbox noise reduction by electrical drive control.* US patent, US8532828B2.

Zhu, Z.Q. and Howe, D. (2000). Influence of design parameters on cogging torque in permanent magnet machines. *IEEE Transactions on Energy Conversion*, 15(4), 407–412. doi:10.1109/60.900501.